Supplementary information

PTPRK regulates glycolysis and *de novo* lipogenesis to promote hepatocyte metabolic reprogramming in obesity

Eduardo H. Gilglioni, Ao Li, Wadsen St-Pierre-Wijckmans, Tzu-Keng Shen, Israel Pérez-Chávez, Garnik Hovhannisyan, Michela Lisjak, Javier Negueruela, Valerie Vandenbempt, Julia Bauzá-Martinez, Jose M. Herranz, Daria Ezeriņa, Stéphane Demine, Zheng Feng, Thibaut Vignane, Lukas Otero Sanchez, Flavia Lambertucci, Alena Prašnická, Jacques Devière, David C. Hay, Jose A. Encinar, Sumeet Pal Singh, Joris Messens, Milos R. Filipovic, Hayley J. Sharpe, Eric Trépo, Wei Wu and Esteban N. Gurzov

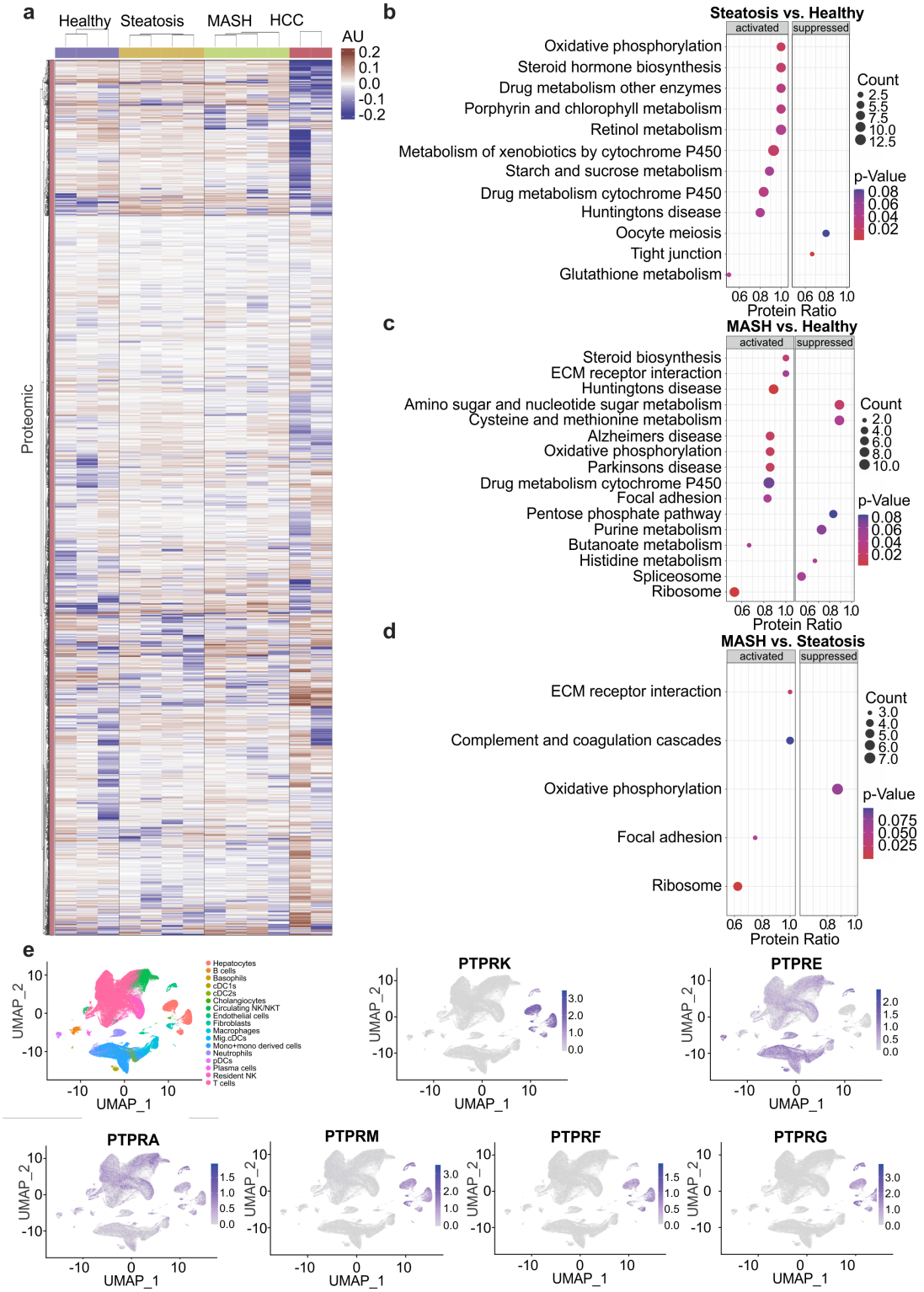

Supplementary Figure 1: Comprehensive liver proteomics, pathway enrichment, and receptor PTPs expression in different hepatic cells. (**a**) Heatmap displaying the hepatic proteome profile. (**b**) Proteomic KEGG pathway enrichment analysis comparing steatosis and healthy livers. (**c**) Proteomic KEGG pathway enrichment analysis comparing MASH and healthy livers. (**d**) Proteomic KEGG pathway enrichment analysis comparing livers with MASH and steatosis. (**e**) Data extracted from GSE192740 showing UMAPs with distinct cell clusters identified in the liver and the distribution of various receptor PTPs across parenchymal and non-parenchymal hepatic cells. In **a-d**, differential expression was performed using EdgeR package after TMM normalization of read counts. p-value was adjusted using Benjamini-Hochberg method. Source data are provided as a Source Data file.

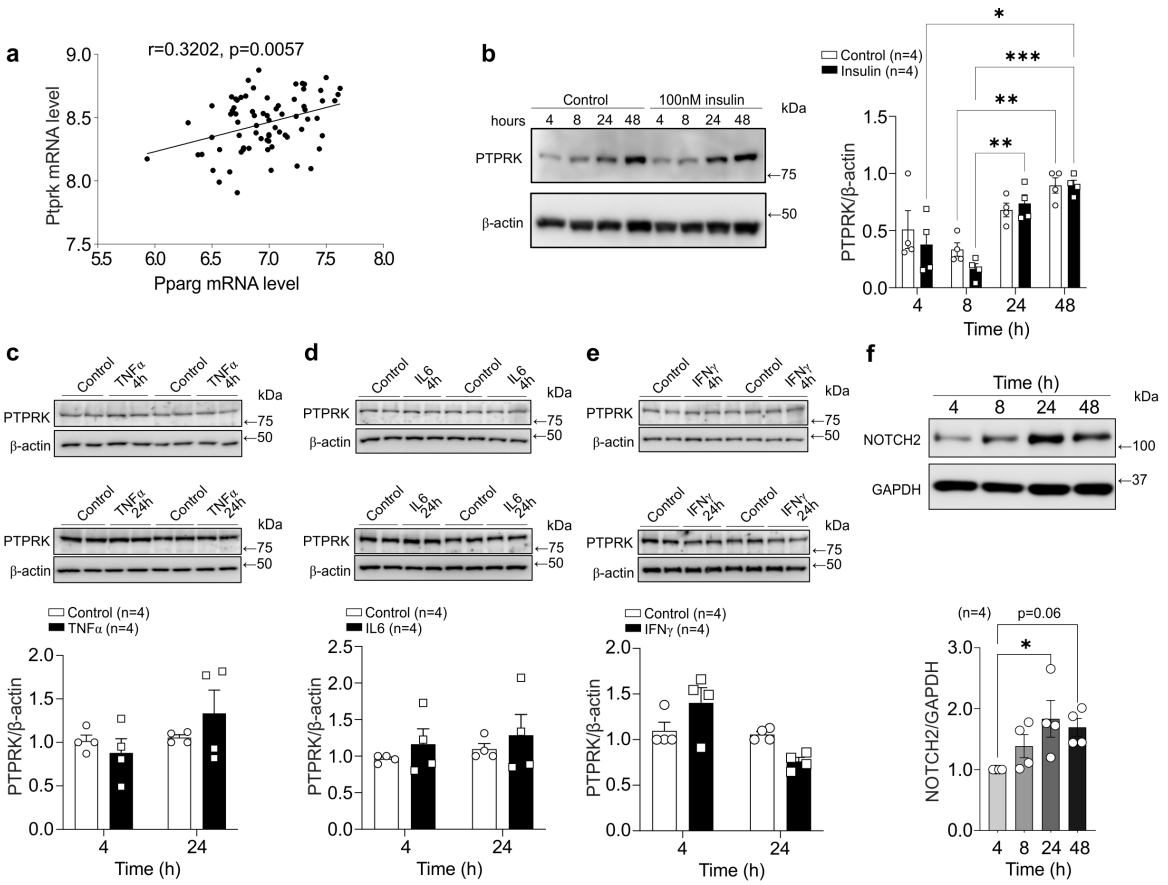

Supplementary Figure 2: Insulin or cytokine treatment does not affect PTPRK expression and culture of primary hepatocytes enhances Notch2 expression. (**a**) Correlation analysis between Ptprk and Pparg mRNA levels in the E-GEOD-48452 dataset. (**b**) Immunoblot analysis of PTPRK expression in mouse primary hepatocytes cultured over time with insulin supplementation. (**c**) Immunoblot analyses of PTPRK expression in mouse primary hepatocytes with acute (4h) and chronic (24h) TNFα treatment. (**d**) Immunoblot analyses of PTPRK expression in mouse primary hepatocytes with acute (4h) and chronic (24h) IL6 treatment. (**e**) Immunoblot analyses of PTPRK expression in mouse primary hepatocytes with acute (4h) and chronic (24h) IFNγ treatment. (**f**) Immunoblot analyses of NOTCH2 expression in mouse primary hepatocytes over time in culture. The presented data represents the average of multiple independent experiments. In **b**-**f** results are shown as means ± SEM. Statistical analyses were done using two-way ANOVA (**b**-**e**) or two-tailed unpaired Student´s t test (**f**). Correlation analyses were performed by using the Spearman rank-correlation test (**a**). Statistical significance is indicated as *p < 0.05, **p < 0.01, ***p < 0.001. Source data are provided as a Source Data file.

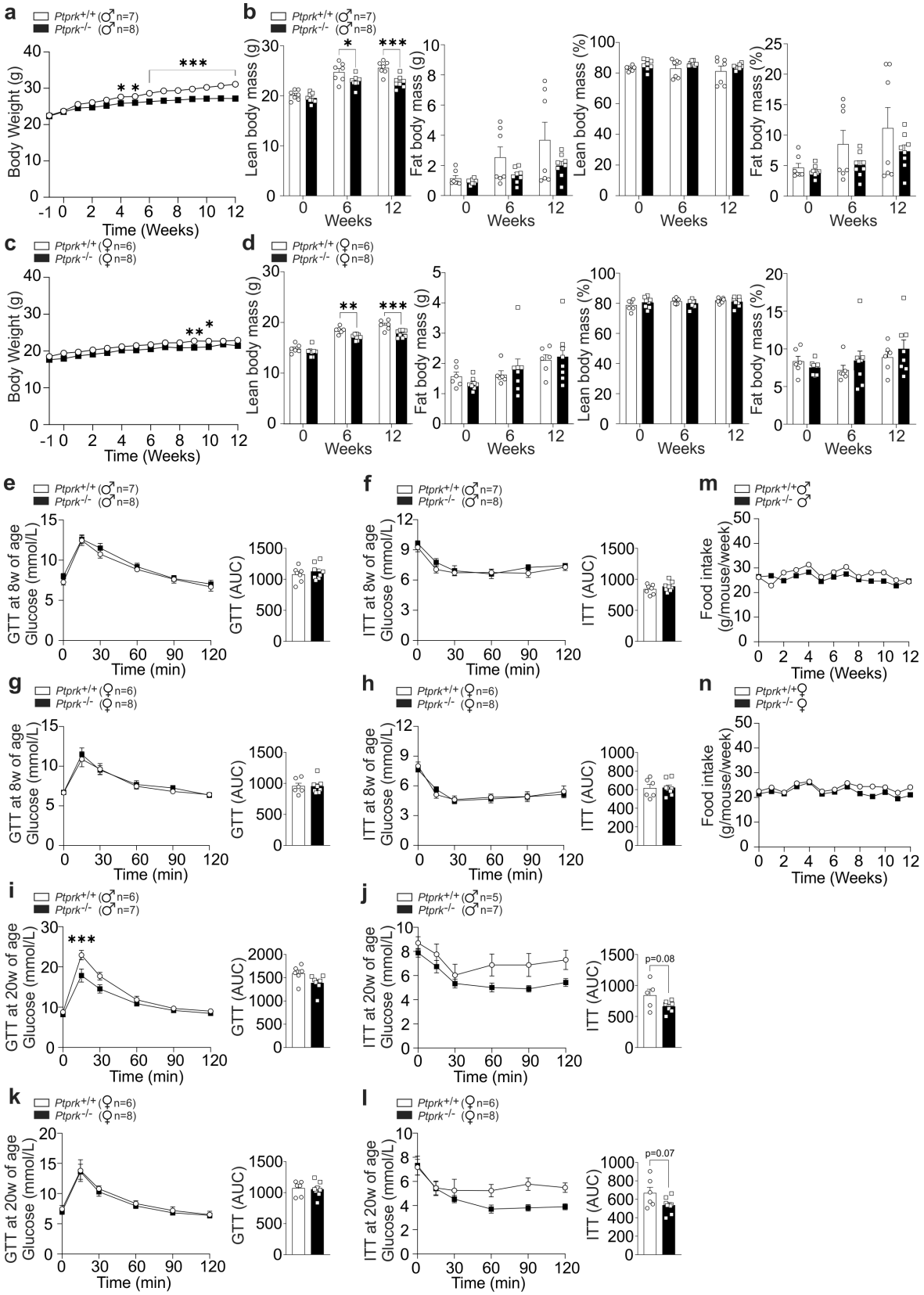

Supplementary Figure 3: Metabolic phenotype shows minor differences in body weight and composition in *Ptprk*$^{-/-}$ and *Ptprk*$^{+/+}$ mice fed a chow diet.

(**a**) Male (♂) *Ptprk*$^{-/-}$ and *Ptprk*$^{+/+}$ C57BL6N mice aged eight weeks were fed a chow diet for 12 weeks, and body weight was measured weekly. (**b**) Body composition in male mice. (**c**) Female (♀) *Ptprk*$^{+/+}$ and *Ptprk*$^{-/-}$ C57BL6N mice aged eight weeks were continuously fed a chow diet for 12 weeks, and body weight was measured weekly. (**d**) Body composition of

female mice. (**e**) Glucose tolerance tests in male mice at 8 weeks of age. (**f**) Insulin tolerance tests in male mice at 8 weeks of age. (**g**) Glucose tolerance tests in female mice at 8 weeks of age. (**h**) Insulin tolerance tests in female mice at 8 weeks of age. (**i**) Glucose tolerance tests in male mice at 20 weeks of age. (**j**) Insulin tolerance tests in male mice at 20 weeks of age. (**k**) Glucose tolerance tests in female mice at 20 weeks of age. (**l**) Insulin tolerance tests in female mice at 20 weeks of age. (**m**) Food intake in male mice. (**n**) Food intake in female mice. In **a-l** results are shown as means ± SEM. Statistical analyses were done using two-tailed unpaired Student's t-test (**e-l**) or using two-way ANOVA (**a-d**). Statistical significance is indicated as *$p < 0.05$, **$p < 0.01$, ***$p < 0.001$, or exact p-value. Source data are provided as a Source Data file.

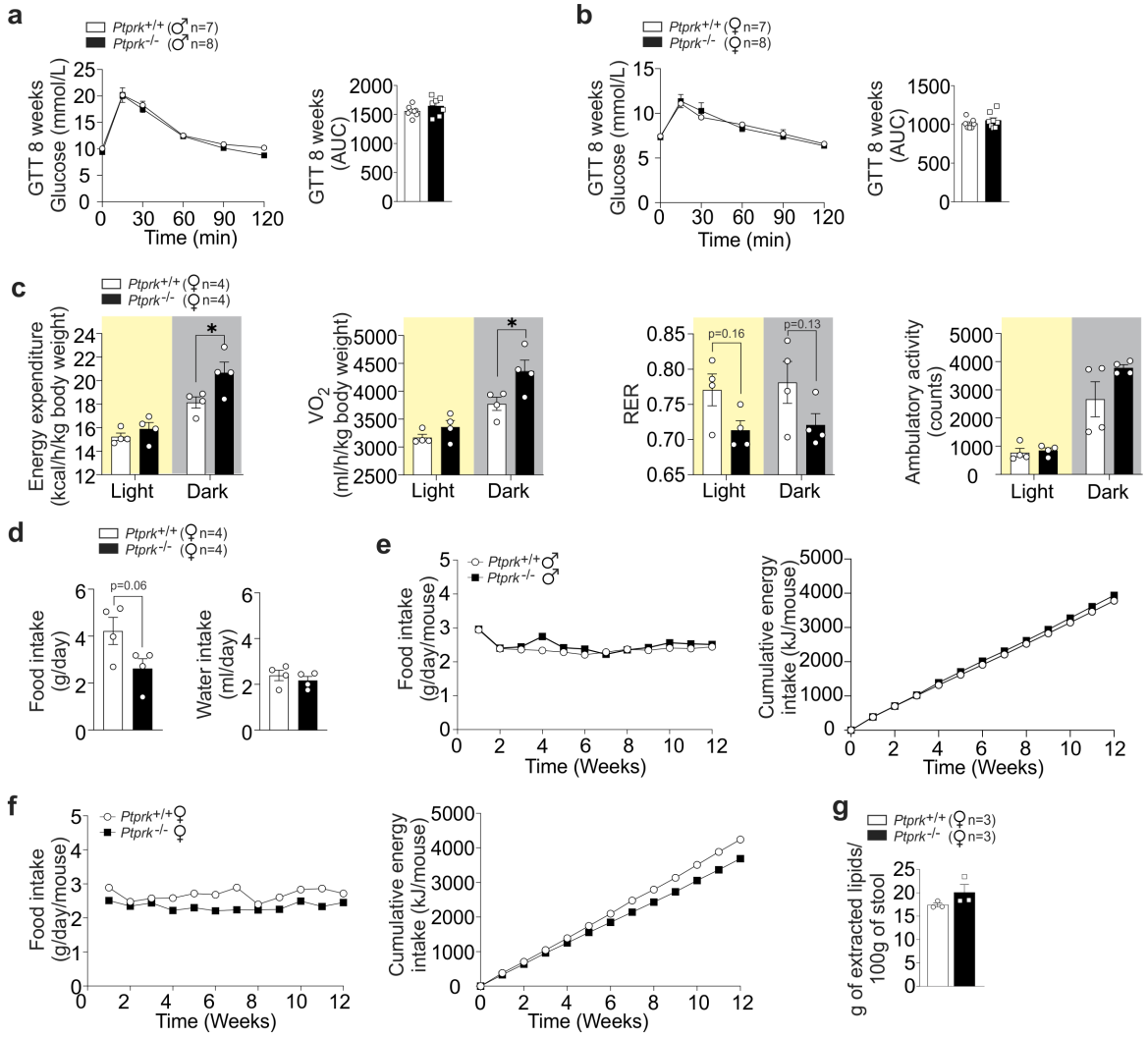

Supplementary Figure 4: Metabolic assessments in *Ptprk*$^{-/-}$ and *Ptprk*$^{+/+}$ mice fed a high-fat, high-fructose, high-cholesterol diet. (**a, b**) Glucose tolerance test performed in male (**a**) and female (**b**) mice at 8 weeks of age (before the HFHFHCD feeding). (**c**) Energy expenditure, oxygen consumption (VO_2), respiratory exchange ratio ($RER=VCO_2/VO_2$) and ambulatory activity measurements in female *Ptprk*$^{+/+}$ and *Ptprk*$^{-/-}$ mice after HFHFHCD feeding for 10 weeks. (**d**) Daily food and water intake in female *Ptprk*$^{+/+}$ and *Ptprk*$^{-/-}$ mice (**e**) Average food intake and cumulative energy intake analyses in male mice fed HFHFHCD. (**f**) Average food intake and cumulative energy intake analyses in females fed HFHFHCD. (**g**) Lipid extraction from stool samples collected over three consecutive days before the end of the 12-week HFHFHCD feeding experimental period in female mice. In **a**-**d**, **g** results are shown as means ± SEM. Statistical analyses were done using two-tailed unpaired Student´s t-test (**a**-**d**, **g**). Statistical significance is indicated as *$p < 0.05$, or exact p-value. Source data are provided as a Source Data file.

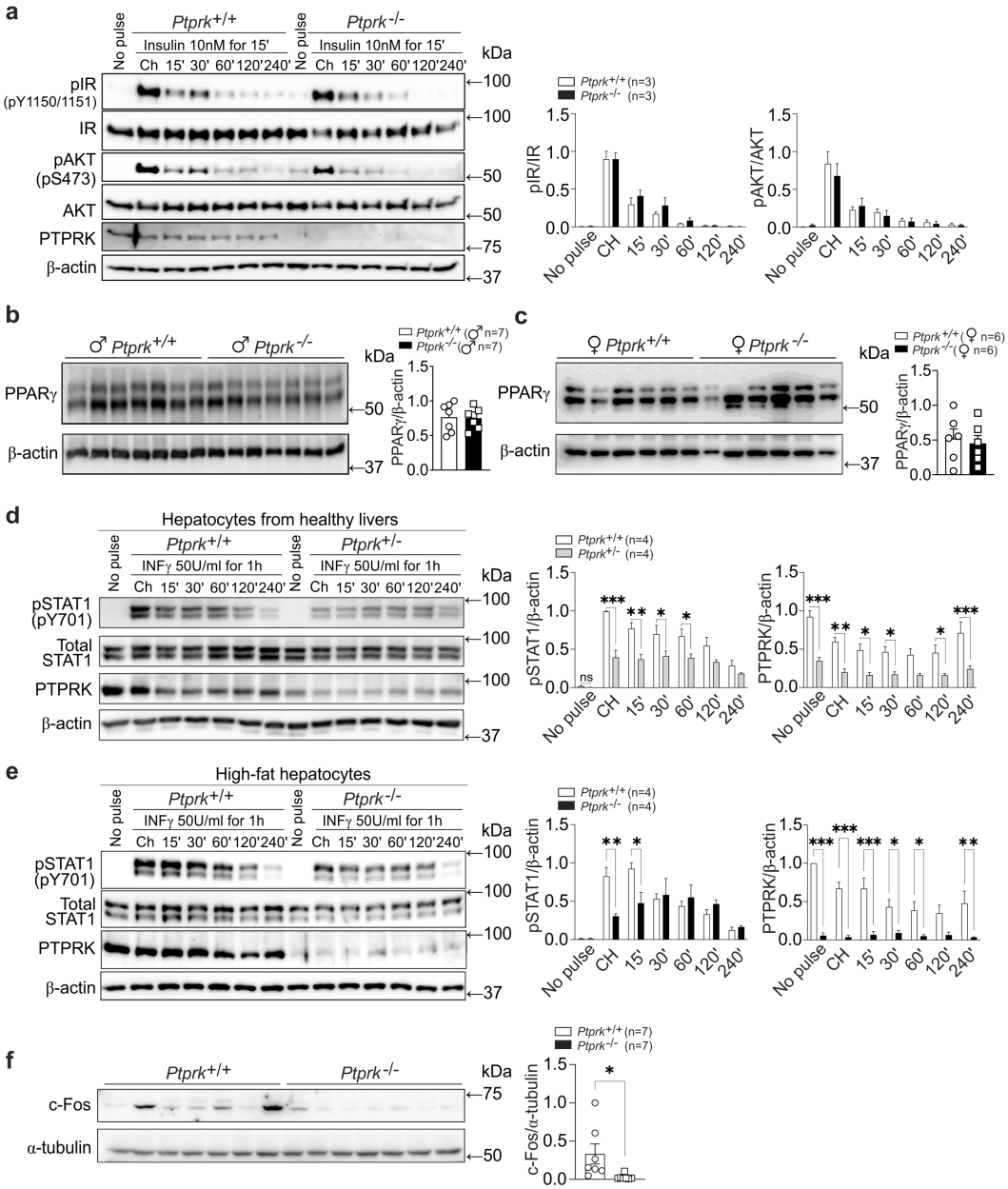

Supplementary Figure 5: Effect of PTPRK on insulin signalling, IFNγ-induced STAT1 activation and hepatic c-Fos expression. (**a**) Immunoblot analysis of pIR, IR, pAKT, AKT, and PTPRK in hepatocytes isolated from *Ptprk*$^{-/-}$ and *Ptprk*$^{+/+}$ mice cultured overnight and subjected to insulin pulse (10 nM for 15 min) and chase (Ch) experiments. (**b, c**) Visceral epididymal (males, **b**) and uterine (females, **c**) white adipose tissues were collected from *Ptprk*$^{-/-}$ and *Ptprk*$^{+/+}$ mice after 12 weeks of HFHFHCD feeding and proteins were extracted for immunoblot analysis of PPARγ. (**d**) Immunoblot analysis showing lower PTPRK levels associated with decreased pSTAT1 activation in response to IFNγ in *Ptprk*$^{+/-}$ and *Ptprk*$^{+/+}$ hepatocytes after a 1h exposure to 50 U/ml IFNγ. (**e**) Immunoblot analysis demonstrates the suppression of IFNγ-induced STAT1 activation in *Ptprk*$^{-/-}$ and *Ptprk*$^{+/+}$ hepatocytes with high-fat content isolated from steatotic livers of male mice at 14 weeks of age following a 1-hour exposure to 50 U/ml IFNγ. (**f**) c-Fos expression was assessed by immunoblot analysis in livers from female *Ptprk*$^{-/-}$ and *Ptprk*$^{+/+}$ mice fed a HFHFHCD for 12 weeks. The presented data represent the average of multiple independent experiments. In **a-f** results are shown as means ± SEM. Statistical analyses were done using two-way ANOVA (**a**, **d**, **e**) or two-tailed unpaired Student´s t-test (**b**, **c**, **f**). Statistical significance is indicated as *p < 0.05, **p < 0.01, ***p < 0.001. Source data are provided as a Source Data file.

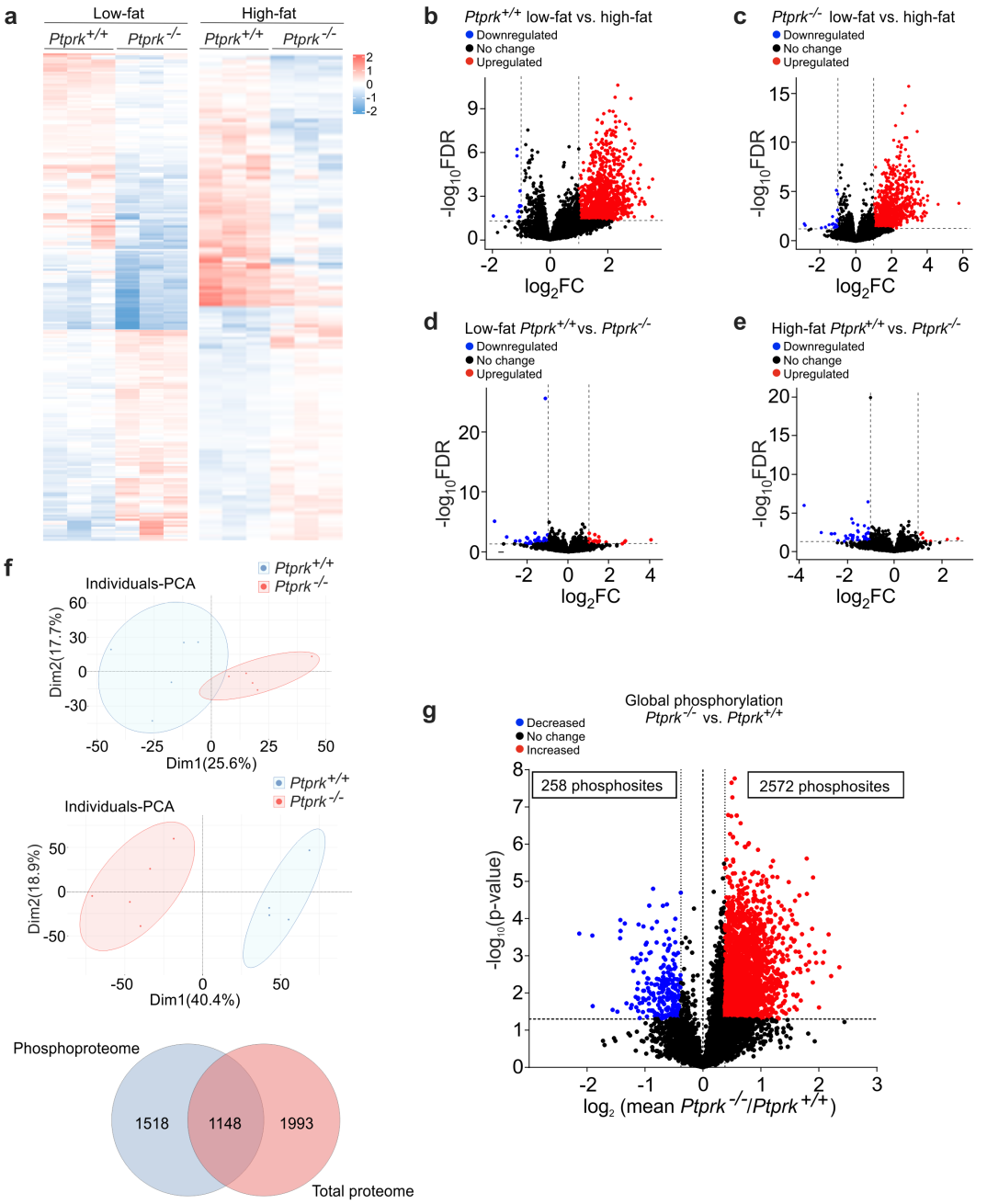

Supplementary Figure 6: Transcriptome, proteome, and protein phosphorylation assays in primary mouse hepatocytes isolated from *Ptprk*$^{-/-}$ and *Ptprk*$^{+/+}$ mice. (**a**) RNA-Seq heatmap showing alterations in mRNA expression in hepatocytes with low- and high-fat content. (**b**) Volcano plot demonstrating the quantification of transcripts in high-fat and low-fat *Ptprk*$^{+/+}$ hepatocytes. (**c**) Volcano plot demonstrating the quantification of transcripts in high-fat and low-fat *Ptprk*$^{-/-}$ hepatocytes. (**d**) Volcano plot displaying the quantification of transcripts between *Ptprk*$^{+/+}$ and *Ptprk*$^{-/-}$ hepatocytes with low fat content. (**e**) Volcano plot displaying the quantification of transcripts between *Ptprk*$^{+/+}$ and *Ptprk*$^{-/-}$ hepatocytes with high-fat content. (**f**) PCA analysis depicting changes in the total proteome (top part) and phosphoproteome (middle part) in *Ptprk*$^{+/+}$ and *Ptprk*$^{-/-}$ hepatocytes. Principal component analysis (PCA) examination revealed that the PCA scores for PC1 (Dim1) and PC2 (Dim2) generated a biplot that segregated into two distinct groups. PC1 and PC2 collectively explained 43.3% of the variability between *Ptprk*$^{-/-}$ and *Ptprk*$^{+/+}$ samples, with PC1 accounting for 25.6% and PC2 for 17.7% of the variance, respectively. A similar analysis for the

phosphoproteomics data showed a more pronounced difference, with PCA scores for PC1 (Dim1) and PC2 (Dim2) producing a biplot that distinctly separated two groups. In this case, PC1 and PC2 together explained 59.3% of the variability between *Ptprk*$^{-/-}$ and *Ptprk*$^{+/+}$ samples, with PC1 contributing 40.4% and PC2 contributing 18.9% of the variance. One group comprised *Ptprk*$^{+/+}$ hepatocytes, while the other group consisted of *Ptprk*$^{-/-}$ hepatocytes, both showing strong alignment along PC2. Venn diagram illustrating proteins identified in the phosphoproteome and total proteome (bottom part). (**g**) Volcano plot showing the quantification of phosphosites between *Ptprk*$^{-/-}$ and *Ptprk*$^{+/+}$ hepatocytes with high-fat content. In **b**-**e**, raw data was processed by DESeq2 and statistical analysis performed by the binomial Wald test, two-sided p-values adjusted with Benjamini-Hochberg method. In **g**, Welch's two-sided t-test was used, and p-value was adjusted using the Permutation based FDR method with 250 randomizations. Source data are provided as a Source Data file.

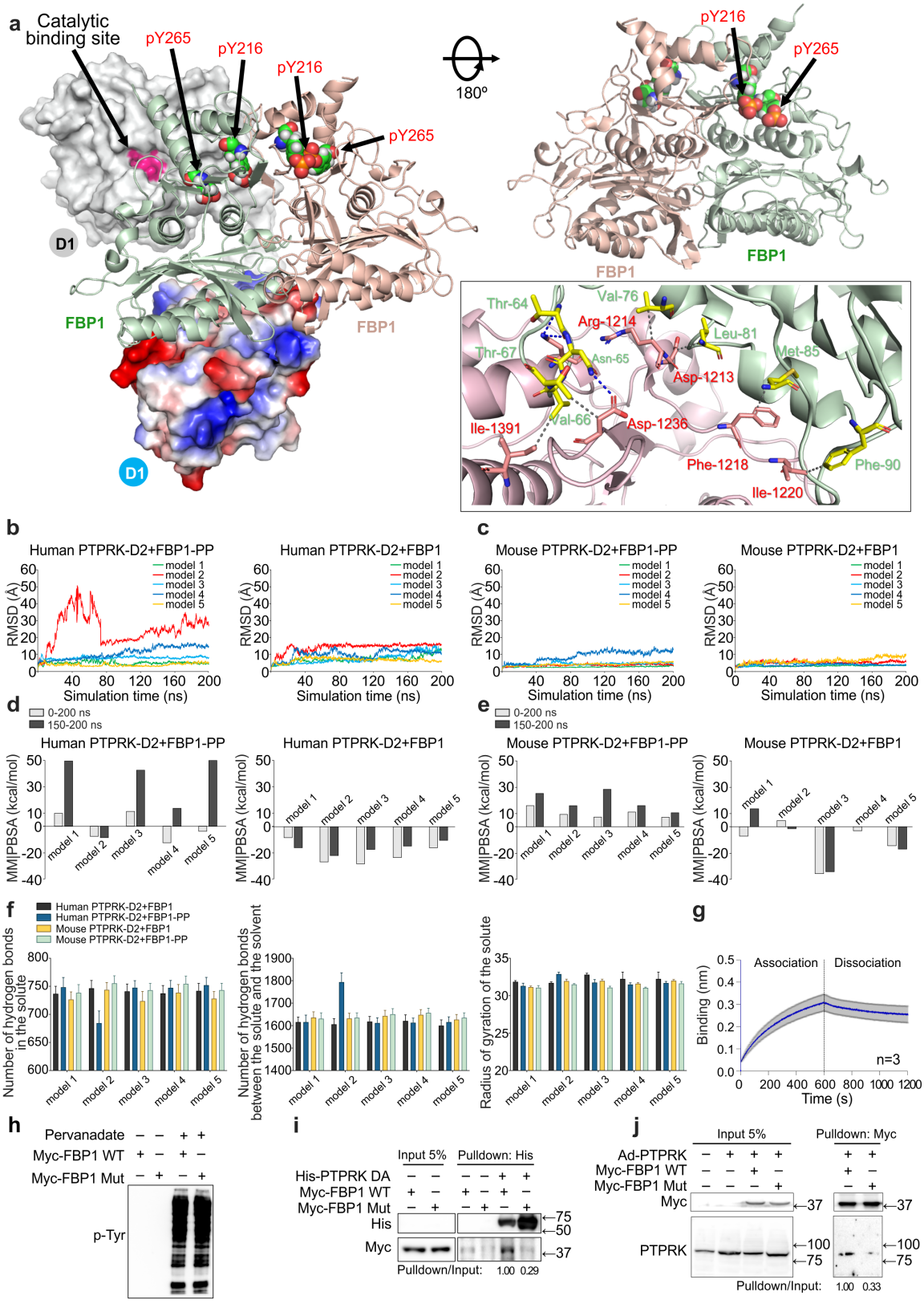

Supplementary Figure 7: Computational and Experimental Analysis of the PTPRK-FBP1 Interaction. (**a**) Structural prediction of the PTPRK-D2:FBP1 phosphorylated dimer complex after 200 ns of molecular dynamics simulation. The electrostatic potential coloured surface of PTPRK-D2, and the polypeptide backbone of the FBP1-pY216, pY265 dimer are shown (light green and light pink). In addition, an open model of PTPRK-D1-D2 (D1 shows the molecular surface in grey) has been superimposed to highlight the proximity of the catalytic site of PTPRK-D1 and the pY216, pY265 residues (represented as spheres) and front

view from the catalytic site of PTPRK-D1 representing the surface of each FBP1 monomer (light green and light pink), where the solvent accessible position of the phosphate groups of residues pY216, pY265 (spheres) is highlighted. At the right bottom part of panel **a**, PTPRK-D2:FBP1 interface (backbone) is shown and the amino acids (sticks) that stabilize the interaction of the complex are highlighted. (**b**-**c**) The RMSD values in Å for the five interaction models calculated during the 200 ns MD simulation for human PTPRK (**b**) and mouse PTPRK (**c**). (**d**, **e**) Solvation binding energy (MM|PBSA, Kcal/mol) values are presented for the simulation time intervals of 0-200 and 150-200 ns, for the PTPRK-D2:FBP1 dimer complex, for both phosphorylated (PP-FBP1, pY265 and pY245) and non-phosphorylated FBP1, in human (**d**) and mouse (**e**) protein. (**f**) Number of H-bonds between the amino acids of the PTPRK-D2:FBP1 dimer complex, number of H-bonds between all amino acids of the PTPRK-D2:FBP1 dimer complex with the solvent and radius of gyration of the solute calculated as the mean ± SD during the 200 ns of MD simulation. (**g**) Human His-FBP1 and a His-tagged nonspecific protein of 22 kDa (negative control) were immobilized onto Octet-NTA biosensors. A wavelength shift (nm) was recorded after incubation with PTPRK at a concentration of 200 nM for 10 min. Subsequently, the protein-bound biosensor was incubated in buffer to measure the dissociation reaction, with background subtraction performed to remove nonspecific binding of PTPRK to the immobilized FBP1. The result is the mean ± SEM of 3 independent experiments. (**h**) HepG2 cells were transfected with either human FBP1-myc wild-type or a triple tyrosine mutant (Y216F, Y245F, and Y265F). Western blot showing increased tyrosine phosphorylation in pervanadate-treated samples. (**i**) Recombinant PTPRK pulldown assay. HepG2 cells were transfected with either human wild-type (WT) or a triple tyrosine mutant (Mut, Y265F, Y245F, Y216F). Pervanadate-treated HepG2 lysates were incubated with purified recombinant His.TEV.Avi.PTPRK ICD D1057A conjugated to pre-washed Ni-Sepharose His-tagged protein resin at room temperature for 1h on a rotor, followed by immunoblotting with indicated antibodies. The result is representative of 2 independent experiments. (**j**) HepG2 cells were transduced with an adenoviral vector to induce PTPRK overexpression (Ad-PTPRK) and then transfected with either human FBP1-myc wild-type (WT) or a triple tyrosine mutant (Mut, Y265F, Y245F, Y216F). Pervanadate-treated cells were lysed and immunoprecipitated with anti-Myc magnetic beads, followed by immunoblotting with indicated antibodies. The result is representative of 2 independent experiments. Source data are provided as a Source Data file.

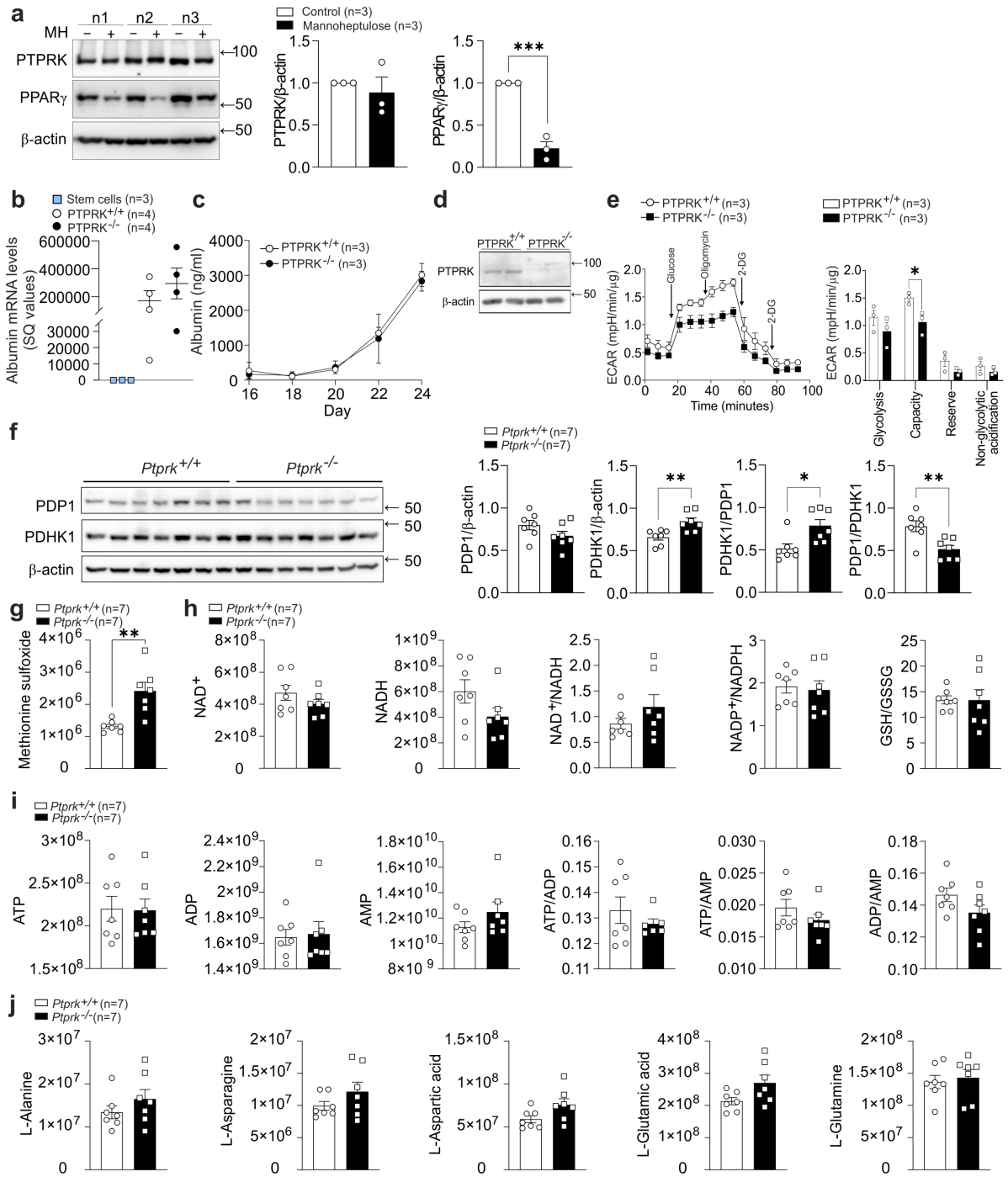

Supplementary Figure 8: Metabolic profiling of *PTPRK*$^{-/-}$ and *PTPRK*$^{+/+}$ human stem cell-derived hepatocyte-like cells and metabolite analysis in livers from *Ptprk*$^{-/-}$ and *Ptprk*$^{+/+}$ mice. (**a**) Primary mouse hepatocytes after overnight in culture were exposed to 24h mannoheptulose (MH) as indicated and PTPRK and PPARγ were assessed by immunoblot. (**b**) Human embryonic stem cells underwent CRISPR-Cas12a editing to delete PTPRK and were differentiated into hepatocyte-like cells. Albumin mRNA levels were measured in stem cells, *Ptprk*$^{+/+}$, and *Ptprk*$^{-/-}$ hepatocyte-like cells. (**c**) Albumin levels were quantified over the course of the differentiation process using ELISA. (**d**) Immunoblot analysis of PTPRK was performed after differentiation into hepatocyte-like cells. (**e**) Glycolysis stress test perfotmrf in *PTPRK*$^{-/-}$ and *PTPRK*$^{+/+}$ hepatocyte-like cells. Real-time measurements of the extracellular acidification rate (ECAR) in response to glycolytic modulators were recorded. The ECAR results were normalized by protein content. (**f**) Liver samples from *Ptprk*$^{-/-}$ and *Ptprk*$^{+/+}$ female mice fed a 12-weeks HFHFHCD were extracted and processed for immunoblot analysis to evaluate the expression of PDP1 and PDHK1. (**g-i**) Livers were harvested from *Ptprk*$^{-/-}$ and

Ptprk$^{+/+}$ female mice fed a 12-week HFHFHCD and metabolite analysis was conducted using mass spectrometry: (**g**) methionine sulfoxide, (**h**) redox status indicators NAD^+, NADH, $NADP^+$/NADPH and reduced glutathione (GSH) to oxidized glutathione (GSSG) ratios (**i**) energy status indicators ATP, ADP, AMP, and their ratios and (**j**) levels of amino acids. Metabolites are presented as raw abundances corrected for liver sample weight. The presented data represent the average of multiple independent experiments. In **a-c**, **e-j** results are shown as means ± SEM. Statistical analyses in **a-c**, **e-j** were done using two-tailed unpaired Student´s t-test. Statistical significance is indicated as *$p < 0.05$, **$p < 0.01$, ***$p < 0.001$. Source data are provided as a Source Data file.

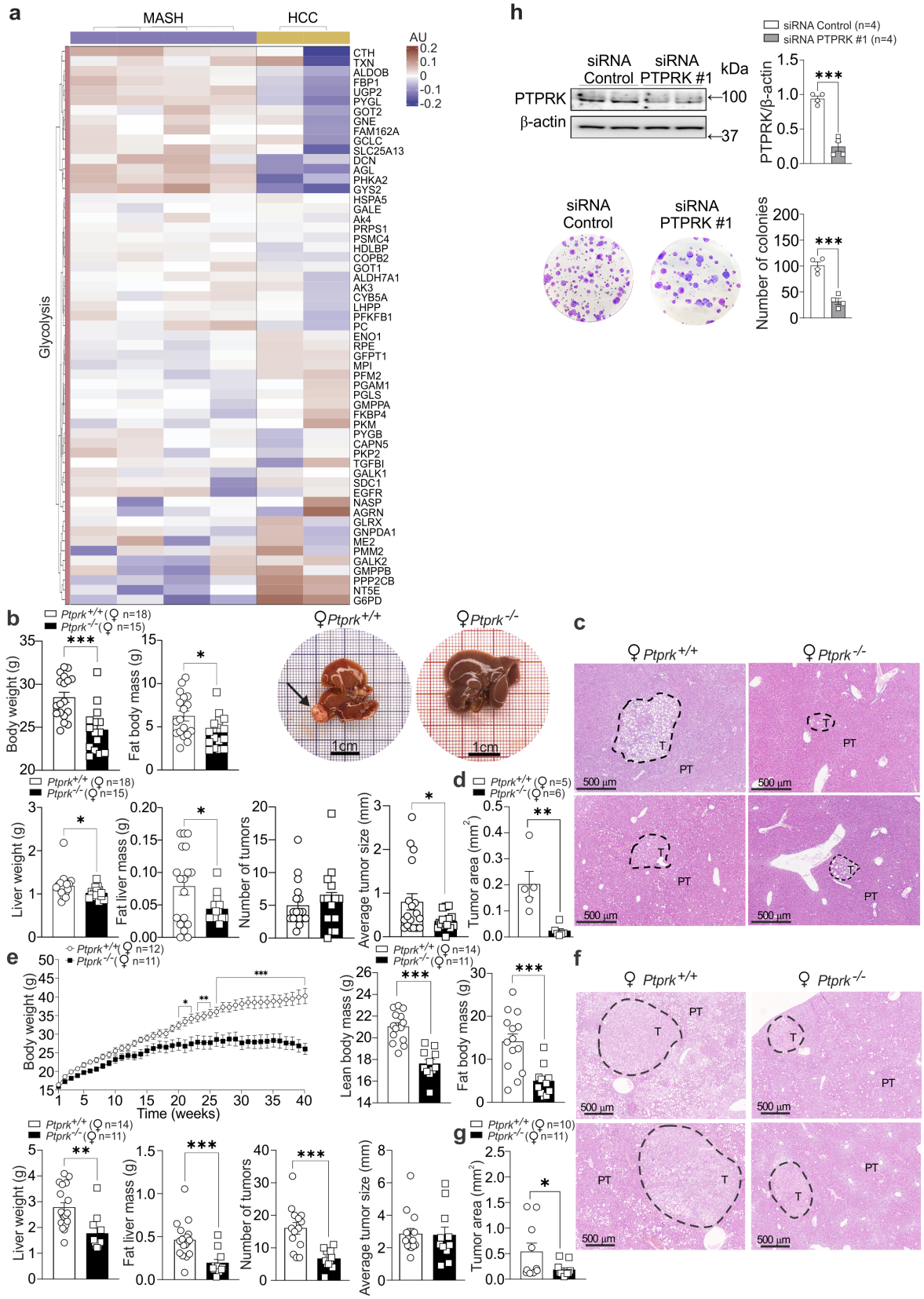

Supplementary Figure 9: Expression of glycolysis-related proteins in MASH and HCC human liver samples, tumour development in female mice, and PTPRK knockdown effects in hepatoma cells. (**a**) Heatmaps were generated to illustrate the expression of proteins involved in glycolysis/gluconeogenesis in human liver samples from individuals with NASH or HCC. (**b-g**) Female *Ptprk*$^{-/-}$ and *Ptprk*$^{+/+}$ mice were subjected to diethylnitrosamine (DEN) induction of liver cancer at 2 weeks of age. (**b-d**) Mice were fed a chow diet and tumour

development was assessed when the animals reached 40 weeks of age. (**e**-**g**) Female *Ptprk*$^{-/-}$ and *Ptprk*$^{+/+}$ mice were fed a HFHFHCD at 6 weeks of age, and tumour harvesting was performed after 40 weeks of feeding, at 46 weeks of age. Measurements of body weight, fat body mass, liver weight, and fat liver mass were recorded. Tumours on the surface of the hepatic lobes were counted and measured, considering tumours larger than 0.2mm. The results are presented as the number of tumours per liver and average tumour size (**b**, **e**). Tumour area measurements were performed using hematoxylin-eosin-stained paraffin-embedded liver sections of the left lobe for the identification and measurement of the area of microtumours within the hepatic lobe. Representative hematoxylin-eosin-stained sections show the presence of nodules, scale bar = 500 μm (**c**, **f**) and tumour area (**d**, **g**). (**h**) Huh6 cells were transfected with siRNA targeting PTPRK or siRNA control. Transfection efficiency was confirmed by immunoblot analysis, and colony-forming capacity was assessed using crystal violet staining for colony number counting (n=4). In **b**, **d**, **e**, **g**, **h** results are shown as means ± SEM. Statistical analyses were done using two-tailed unpaired Student´s t-test (**b**, **d**, **e**, **g**, **h**). Statistical significance is indicated as *$p < 0.05$, **$p < 0.01$, ***$p < 0.001$. Source data are provided as a Source Data file.

ID	Biopsy health status	Age	Weight (kg)	Height (cm)	BMI (kg/m^2)	Type 2 diabetes	Gender	Steatosis score	Fibrosis	Experiment
CHR01	Healthy liver	80	46	175	15	No	M	0	F0	MS/IHC
CHR02	Healthy liver	66	62	150	28	No	F	0	F0	MS/IHC
CHR03	Healthy liver	28	66	170	23	No	F	0	F0	IHC
CHR04	Healthy liver	63	66	165	24	No	F	0	F0	MS/IHC
CHR08	Steatosis	53	86	185	25	Yes	F	2	F0	MS/IHC
CHR09	Steatosis	39	80	158	32	No	F	1	F0	MS/IHC
CHR10	Steatosis	56	67	173	22	No	M	1	F0	MS/IHC
CHR11	Steatosis	36	82	160	32	No	F	1	F0	MS/IHC
CHR12	Steatosis	61	76	159	30	No	F	2	F0	IHC
CHR13	Steatosis	68	115	168	41	Yes	M	1	F0	IHC
CHR14	MASH/cirrhosis	61	113	179	35	Yes	M	1	F4	MS/IHC
CHR16	MASH/cirrhosis	46	79	156	32	No	F	2	F4	MS/IHC
CHR17	MASH/cirrhosis	48	76	160	30	No	M	2	F4	MS/IHC
CHR18	MASH/cirrhosis	60	80	149	36	Yes	F	1	F4	MS/IHC
CHR19	MASH	46	80	157	32	Yes	F	3	F1	MS
CHR20	MASH	45	85	156	35	Yes	F	2	F1	MS
CHR05	HCC	83	79	175	26	No	M	1	F4	MS
CHR06	HCC	76	76	165	28	No	M	1	F0	MS
CHR07	HCC	43	43	170	19	No	M	0	F4	MS

Supplementary table 1: Clinical and demographic characteristics of patients from whom liver biopsies were collected and used for mass spectrometry (MS) or PTPRK immunohistochemistry (IHC) analysis shown in Figure 1. The steatosis score is based on NAS score criteria. The fibrosis and steatosis score were based on the criteria defined Kleiner DE, et al. (doi.org/10.1002/hep.20701).

siRNA	Source or reference	Identifiers	Sense (5´->3´)	Antisense (5´->3´)
siRNA PTPRK #1	Ambion by Life Technologies	s11559	CCAGUAGCCCAG ACUAAGAtt	UCUUAGUCUGGG CUACUGGta
siRNA PTPRK #2	Ambion by Life Technologies	s11558	CAGCUAUAGCAG UAUAAGAtt	UCUUAUACUGCUA UAGCUGat
siRNA PPARg	Quiagen	SI01385391	GCCAUUCCUUUG ACAUCAAtt	UUGAUGUCAAAG GAAUGCGag
siRNA Control	Quiagen	1027281	-	-

Supplementary table 2: List of siRNAs used for RNA interference in the present study.

Antibody	Designation	Source or reference	Identifiers	Additional information
β-actin	Mouse monoclonal anti-beta-actin	Sigma-Aldrich	Cat# A1978	Western blot 1:5000
GAPDH	Rabbit polyclonal anti-glyceraldehyde-3-phoshphate dehydrogenase	R&D Systems	Cat# 2275-PC-100	Western blot 1:5000
α-tubulin	Mouse monoclonal anti-alpha-tubulin	Sigma-Aldrich	Cat# T5168	Western blot 1:5000
Vinculin	Rabbit polyclonal anti-vinculin	Cell Signaling Technology	Cat# 4650	Western blot 1:1000
pY	Mouse monoclonal anti-phospho-tyrosine antibody	Cell Signaling Technology	Cat# 9411	IP 1:50 Western blot 1:1000
PTPRK	Human monoclonal anti-PTPRK	Fearnley et al. 2019, Kindly provided by Hayley Sharpe	2 .H4	Western blot 1:1000
PTPRK	Rabbit polyclonal anti-PTPRK	Thermo Fisher Scientific	Cat# PA5-104089	IHC 1:100
PPARγ	Rabbit monoclonal anti- PPARγ	Cell Signaling Technology	Cat# 2443	Western blot 1:500
pIR	Rabbit monoclonal anti-phospho-IGF-I Receptor β (Tyr1135/1136)/Insulin Receptor β (Tyr1150/1151)	Cell Signaling Technology	Cat# 3024S	Western blot 1:500
IR	Rabbit monoclonal anti-Insulin Receptor β	Cell Signaling Technology	Cat# 3025	Western blot 1:1000
pAKT	Rabbit monoclonal anti-phospho-AKT (Ser473)	Cell Signaling Technology	Cat# 4060	Western blot 1:1000
AKT	Mouse monoclonal anti-AKT (pan)	Cell Signaling Technology	Cat# 2920S	Western blot 1:1000
ACC	Mouse monoclonal anti-acetyl CoA carboxylase	Cell Signaling Technology	Cat# 3676S	Western blot 1:1000
FASN	Rabbit monoclonal anti-fatty acid synthase	Cell Signaling Technology	Cat# 3180S	Western blot 1:1000
SREBP1	Mouse monoclonal anti-sterol regulatory element binding protein 1	Santa Cruz Biotechnology	Cat# sc-13551	Western blot 1:1000
ChREBP1α	Rabbit polyclonal anti-Carbohydrate-responsive element-binding protein alpha	Cell Signaling Technology	Cat# 58069	Western blot 1:1000
pFBP1 (Y265)	Rabbit polyclonal anti-Phospho-fructose 1,6 bisphosphatase 1 (Tyr265)	Thermo Fisher Scientific	Cat# PA5-105335	Western blot 1:1000
FBP1	Rabbit polyclonal anti-fructose 1,6 bisphosphatase 1	Cell Signaling Technology	Cat# 59172	Western blot 1:1000
PDP1	Rabbit monoclonal anti-pyruvate dehydrogenase phosphatase 1	Cell Signaling Technology	Cat# 65575S	Western blot 1:1000
PDHK1	Rabbit monoclonal anti-pyruvate dehydrogenase kinase 1	Cell Signaling Technology	Cat# 3820S	Western blot 1:1000
c-Fos	Rabbit polyclonal anti-protein c-Fos	Cell Signaling Technology	Cat# 4384S	Western blot 1:1000
Notch2	Rabbit monoclonal anti-Neurogenic locus notch homolog protein 2	Cell Signaling Technology	Cat# 5732S	Western blot 1:1000
pSTAT1	Mouse monoclonal anti-phospho-STAT1 (Y701)	BD-Biosciences	Cat# 612132	Western blot 1:1000
STAT1	Rabbit polyclonal anti-STAT1	Cell Signalling Technology	Cat# 9172S	Western blot 1:1000
His	Mouse monoclonal anti Histidine Tag	Bio-Rad	Cat# MCA1396	Western blot 1:1000
Myc	Mouse monoclonal anti-Myc-Tag	Cell Signaling Technology	Cat# 2276	Western blot 1:1000
HIF-2α	Rabbit monoclonal anti-Hypoxia-inducible factor 2 alpha	Cell Signaling Technology	Cat# 57921S	Western blot 1:500

Supplementary table 3: Antibodies used in the present study.

Gene name	qPCR Fw	qPCR Rv	STD Fw	STD Rv
Tnf	AGGCACTCCCC CAAAAGATG	TGAGGGTCTGGG CCATAGAA	ATGAGCACAGA AAGCATGATC	TACAGGCTTGT CACTCGAATT
Pparγ1	CCAAGAATACCA AAGTGCGATCA	AAAACCCTTGCA TCCTTCACAA	GCTCCAAGAAT ACCAAAGTGCG A	AACCTGATGGC ATTGTGAGACA
Pparγ2	TGCCTATGAGCA CTTCACAAG	TCTACTTTGATC GCACTTTGGTA	AGCATGGTGCC TTCGCTGAT	GCCCAAACCTG ATGGCATTGTG
Cyp7a1	TAAGGAGAAGG AAAGTAGGTGAA C	CCAAATGCCTTC GCAGAAGTAG	TGGAATAAGGA GAAGGAAAGTA GG	TCCAAATGCCTT CGCAGAAGTA
Gapdh	AGTTCAACGGCA CAGTCAAG	TACTCAGCACCA GCATCACC	ATGACTCTACC CACGGCAAG	TGTGAGGGAGA TGCTCAGTG
Fasn	CACAGTGCTCAA AGGACATGCC	CACCAGGTGTAG TGCCTTCCTC	ACTTCCTCTGG GATGTGCCT	GTCAGCACTGC TCTCGTTGA
Pck1	GCAGTGAGGAA GTTCGTGGA	GTGAGAGCCAGC CAACAGT	GCTGCATAACG GTCTGGACT	ATACATGGTGC GGCCTTTCAT
Cd36	TAATGGCACAGA CGCAGC	GGTTGTCTGGAT TCTGGAGGG	TAATGGCACAG ACGCAGC	ACATCACCACT CCAATCCCA
Cpt1α	GCTGATGACGG CTATGGTGT	AAAGCGGTGTGA GTCTGTCT	CCACAACAACG GCAGAGCA	TCAGGAGCAAC ACCTATTCATTT G
Scd1	TGCCGTGGGCG AGGG	ACACCCCGATAG CAATATCCA	TGATGTTCCAG AGGAGGTACTA CA	AATGCATCATTA ACACCCCGA
Ptprk	TCGTGATTGGCT TCGGG	CCAGCATTGACC TCCACA	TGAAGGAGAAT GACACCCAC	TCTGAAAGAGG CAGCAAATCT
Acly	TTCGTCAAACAG CACTTCC	ATTTGGCTTCTT GGAGGTG	ACACCATCATCT GTGCTCGG	ATCCCAGGGGT GACGATACA
Acaca (Acc)	AGCCAGAAGGG ACAGTAGAA	CTCAGCCAAGCG GATGTAAA	GCGCTTACATT GTGGATGGC	AAGCCTTCACT GTGCCTTCA
Actb (β-actin)	ACGGCCAGGTCAT CACTATT	GTTGGCATAGAGGT CTTTACG	AGAGGAAATCGTG CGTGAC	TCTCCTTCTGCAT CCTGTCA
Alb (human)	GAAAAGTGGGC AGCAAATGT	GGTTCAGGACCA CGGATAGA	GAGCAGCTTGG AGAGTACAA	GTTTCAGCATTA AACTCTTT

Supplementary table 4: Primer sequences used for RT-PCR experiments.